CFD SIMULATION OF FLOW AROUND 3D SUBMARINE SHAPED BODY

M. Sharif Khan[1*], Md. Mahbubar Rahman[1] and Md. Mashud Karim[2]

[1] Department of Mathematics, MIST, Mirpur Cantonment, Dhaka-1216, Bangladesh
*E-mail: sharif918590@gmail.com
E-mail: md.mahbubar@gmail.com
[2] Department of Naval Architecture & Marine Engineering, BUET, Dhaka-1000, Bangladesh
E-mail: md.mahbubmashudbuet@gmail.com, mmkarim@name.buet.ac.bd

ABSTRACT

Drag estimation and shape optimization of submarine shaped hulls are important for energy efficiency and hull form improvement. In this study, fluid flow around the 3D DREA bare submarine hull is simulated with the help of finite volume method. Widely implemented Reynolds-averaged Navier-Stokes (RANS) approach and SST k-ω turbulence model with low-Re version are used to represent turbulent transport equations. Computed results are compared with experimental results as well as simulated results of other researchers and found satisfactory. The velocity distribution (vectors, contours and streamlines), pressure distribution and drag coefficient are also analyzed. The result of this study illustrated the flow physics around 3D submarine shaped hull which might be helpful for improvement of design of such underwater bodies.

Key Words: Computational Fluid Dynamics (CFD), Hull Form Optimization, Numerical Simulation, Underwater Vehicle, Turbulence Model, 3D Submarine Shape.

1.0 INTRODUCTION

Computational fluid dynamics constitutes a new approach in the theoretical study and development of the whole discipline of fluid dynamics. Throughout most of the twentieth century the study and practice of the fluid dynamics involved use of the pure theory on one hand and pure experiment on the other hand. The advent of the high-speed digital computers combined with the development of accurate numerical algorithms for solving physical problems on these computers has revolutionized the way we study and practice fluid dynamics today. CFD is a major tool in solving hydrodynamic problems associated with ships, submarines, torpedoes, etc. It can offer cost-effective solution to many problems including underwater vehicle hull forms. The modeling and simulation of an underwater vehicle and calculation of the relevant hydrodynamic coefficients have been performed by many researchers. However, effective utilization of CFD for marine hydrodynamics depends on proper selection of turbulence model, grid generation and boundary conditions. Finite volume method for computation of hydrodynamic forces is based on Reynolds-averaged Navier-Stokes (RANS) equations. Various researchers used turbulence modeling to simulate flow around axisymmetric bodies since late seventies. Patel and Chen [1] made an extensive review of the simulation of flow past axisymmetric bodies. Choi and Chen [2] gave calculation method for the solution of RANS equation, together with k-εturbulence model. *Sarkar et al.* [3] used a low-Re k-ε model of Lam and Bremhorst [4] for simulation of turbulent flow past underwater axisymmetric bodies. Karim *et al.* [5-8] showed that SST k-ω model is more effective to calculate drag force and unstructured grid gives more accurate results than structured grid for the underwater slender bodies. However, these studies were limited to 2D axisymmetric underwater bodies. In this study, SST k-ω (with low-Re version) model is used to simulate fluid flow past 3D DREA bare hull with the help of ANSYS Fluent 16.2 CFD software.

2.1 Mass Conservation Equation

The equation of conservation of mass or continuity equation can be expressed as:

$$\frac{\partial \rho}{\partial t} + \nabla.(\rho \vec{v}) = S_m \quad (1)$$

Equation (1) is the general form of the mass conservation equation and is valid for incompressible as well as compressible flows [9]. The source S_m is the mass added to the continuous phase from the dispersed second phase (for example, due to vaporization of liquid droplets) and any user-defined sources.

2.2 Momentum Conservation Equations

Conservation of momentum in an inertial (non-accelerating) reference frame is described by -

$$\frac{\partial}{\partial t}(\rho \vec{v}) + \nabla.(\rho \vec{v}\vec{v}) = -\nabla p + \nabla.(\bar{\bar{\tau}}) + \rho \vec{g} + \vec{F} \quad (2)$$

where p is the static pressure, $\bar{\bar{\tau}}$ is the stress tensor and $\rho \vec{g}$ and $\vec{F}$ are the gravitational body force and external body forces respectively. $\vec{F}$ is also contains other model-dependent source terms such as porous-media and user-defined sources.

2.3 Shear-Stress Transport (SST) k-ω Model

The SST k-ω turbulence model, developed by Menter in 1993, is a two-equation eddy-viscosity model which has become very popular. The use of a k-ω formulation in the inner parts of the boundary layer makes the model directly usable all the way down to the wall through the viscous sub-layer; hence the SST k-ω model can be used as a low-Re turbulence model without any extra damping functions. The SST formulation also switches to k-ε behavior in the free-stream and thereby avoids the common k-ω problem that the model is too sensitive to the inlet free-stream turbulence properties. The SST k-ω model is similar to the standard k-ω model, but includes the following refinements:

- The standard k-ω model and the transformed k-ε model are both multiplied by a blending function and both models are added together.
- The blending function is designed to be one in the near-wall region, which activates the standard k-ω model and zero away from the surface, which activates the transformed k-ε model.
- The SST model incorporates a damped cross-diffusion derivative term in the ω-equation.
- The definition of the turbulent viscosity is modified to account for the transport of the turbulent shear stress.
- The modeling constants are different.

These features make the SST k-ω model more accurate and reliable for a wider class of flows than the standard k-ω model [8].

Transport equations for the SST k-ω Model are:

$$\frac{\partial}{\partial t}(\rho k) + \frac{\partial}{\partial x_i}(\rho k u_i) = \frac{\partial}{\partial x_i}\left(\Gamma_k \frac{\partial k}{\partial x_i}\right) + G_k - Y_k + S_k \quad (3)$$

and

$$\frac{\partial}{\partial t}(\rho \omega) + \frac{\partial}{\partial x_j}(\rho \omega u_j) = \frac{\partial}{\partial x_j}\left(\Gamma_\omega \frac{\partial k}{\partial x_j}\right) + G_\omega - Y_\omega + D_\omega + S_\omega \quad (4)$$

In these equations, the term G_k represents the production of turbulence kinetic energy and is defined in the same manner as in the standard k-ω model. G_ω represents the generation of ω, calculated as described for the standard k-ω model in Modeling the Turbulence Production. Γ_k and Γ_ω represent the effective diffusivity of k and ω respectively. Y_k and Y_ω represent the dissipation of k and ω due to turbulence. D_ω represents the cross-diffusion term. S_k and S_ω are user-defined source terms.

3.0 METHODOLOGY

A finite volume based CFD package ANSYS Fluent 16.2 is employed to obtain the solution of the Reynolds-averaged Navier-Stokes equations. The pressure based segregated solver was selected, which solves the pressure and momentum sequentially. Semi-Implicit Method for Pressure-Linked Equations (SIMPLE) algorithm is used for coupling between the pressure and velocity fields. Second order upwind interpolation scheme for the convection term was selected for 2nd order

accuracy. Least squares cell based approach is used to determine the gradients of solution variables at cell centers. Second order interpolation scheme is selected for calculating cell-face pressure. An absolute convergence criterion of 10^{-3} is set for all the discretized equations.

3.1 Hull Geometry

In this study, the computational domains are created around the DREA (Defence Research Establishment Atlantic) standard bare submarine hull as used by Department of Research and Development Canada, 1988. The geometry of the hull is considered to stay consistent with the experimental result. The vertices of 2D axisymmetric geometry are created using following formulas:

For nose section,

$$\frac{r_1(x)}{l} = \frac{d}{l}\left[2.56905\sqrt{\frac{x}{l}} - 3.48055\frac{x}{l} + 0.49848\left(\frac{x}{l}\right)^2 + 3.40732\left(\frac{x}{l}\right)^3\right] \quad where, 0 \le \frac{x}{l} \le 0.2 \qquad (5)$$

For mid body,

$$\frac{r_2(x)}{l} = \frac{d}{l} \quad where, \quad 0.2 \le \frac{x}{l} \le 1 - \frac{3d}{l} \qquad (6)$$

For tail section,

$$\frac{r_3(x)}{l} = \frac{d}{2l} - \frac{l}{18d}\left[\frac{x}{l} - \left(1 - \frac{3d}{l}\right)\right]^2 \qquad (7)$$

$$where, \quad 1 - \frac{3d}{l} \le \frac{x}{l} \le 1$$

where, l is the length of the hull, d is the maximum diameter and $l/d = 8.75$. By revolving 2D axisymmetric sketch 360^0 around x-axis 3D DREA bare hull has been created and shown in Fig 1.

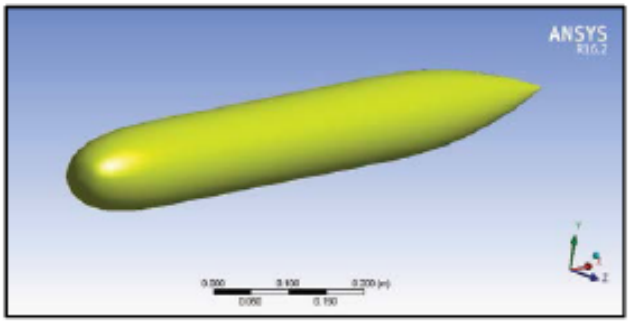

Fig 1: DREA bare submarine hull

3.2 Flow Domain

Fig 2 shows computational domain for this present study. Distances of the inlet and outlet boundary from leading edge of the DREA body are considered $0.25l$ and $2l$ respectively. The sides, top and bottom boundary is located at $0.25l$ from DREA centerline. Since the flow is incompressible, the considered downstream solution domain is ensured large enough to capture the entire viscous-inviscid interaction and wake development.

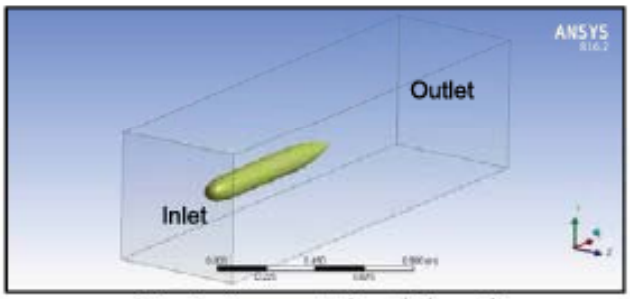

Fig 2: Computational domain

3.3 Mesh Generation

Finite volume method is the common approach to solve RANS equations in the computational domain. Computational domain needs to be discretized to solve discretized RANS equations within them. In this study, unstructured grid is generated by using ANSYS Fluent Meshing software. The mesh was then exported to Fluent Solver for numerical study. Tetrahedral method with patch conforming algorithms used to generate mesh of the flow domain and 3D inflation is also created. Total 1012048 regular elements were built with 272602 nodes in the solution domain. Minimum orthogonal quality is found 4.20×10^{-1}, maximum ortho skew is found 5.42×10^{-1} and maximum aspect ratio is found 9.89, which are in acceptable range.

In order to ensure that sufficient numbers of grid points are used to resolve the boundary layer, the turbulence closure model requires that the wall $y^+ = \frac{yu_\tau}{\nu}$ (where, $u_\tau = \sqrt{\frac{\tau}{\rho}}$ is the friction velocity) parameters must satisfy a certain criterion. Grid points supposed to keep close enough near DREA body in such way that wall $y^+ < 40$ to obtain accurate results using SST k-ω turbulence method [10], which is maintained for the present study. Fig 3 shows y^+ distribution around the body and Fig 4 shows details of generated unstructured mesh of the domain.

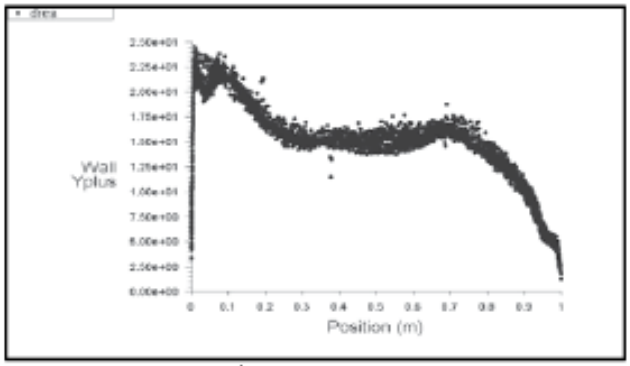

Fig 3: Wall Y^+ distribution around the 3D submarine body

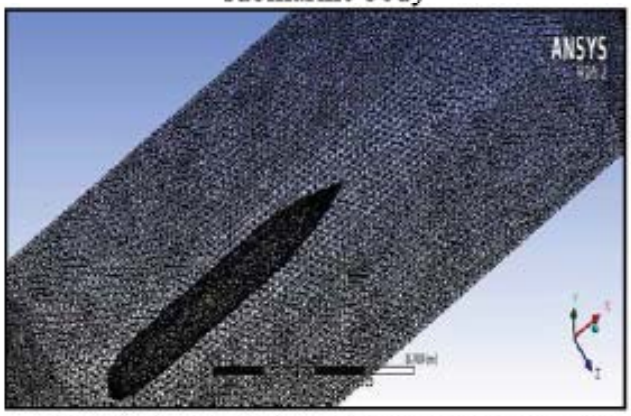

Fig 4(a): Unstructured mesh of the flow domain

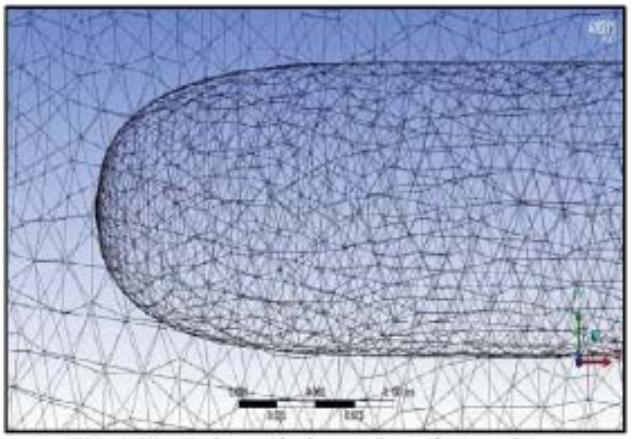

Fig 4(b): Enlarged view of mesh near bow

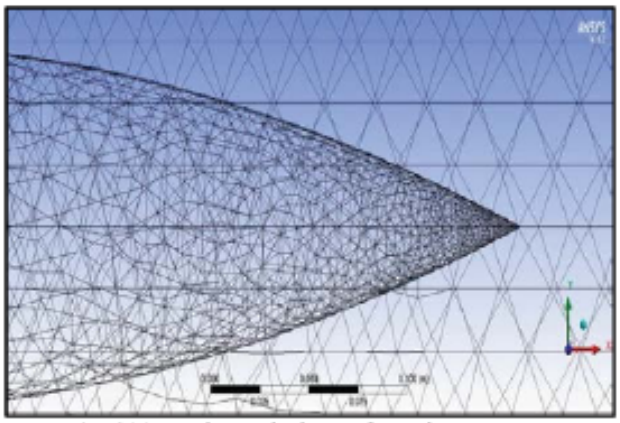

Fig 4(c): Enlarged view of mesh near stern

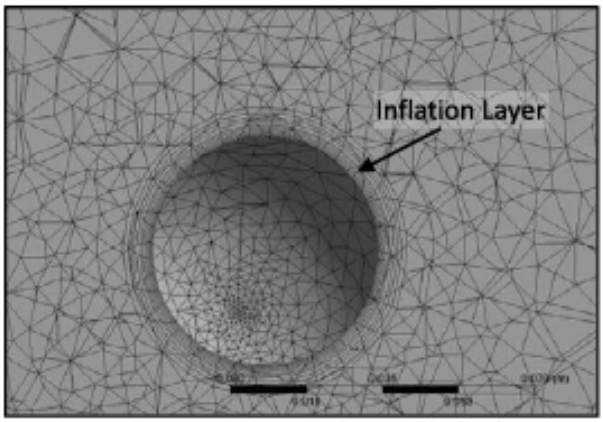

Fig 4(d): Cross sectional view of inflation layer

3.4 Model Selection and Boundary Conditions

Shear Stress Transport (SST) *k-ω* turbulence model is used for capturing turbulent flow. This model combines the accurate near-wall treatment of the *k-ω* method with the free-stream independence of the *k-ε* method by using a blending function; thus it enables the model to switch between the standard *k-ω* model near the wall and standard *k-ε* model in the far-field. Reynolds number (*Re*) value is kept to 23003039 to keep consistency with the experiment. At the upper boundary, free-slip boundary condition is specified $\left(\frac{\partial u}{\partial y} = v = 0\right)$. At the outlet, the outflow boundary condition, given by $\frac{\partial u}{\partial x} = \frac{\partial v}{\partial x} = 0$ with zero turbulence $(k = \omega = 0)$, is imposed. At the solid wall of the hull, the widely used wall boundary conditions $(u = v = 0)$ are used. All other parameters are kept in model default value.

4.0 MODEL VALIDATION

The 2D axisymmetric geometry of the DREA bare hull is selected for the purpose of validating the numerical model. Obtained results are found

satisfactory, as shown in Table 1, compared to the CFD results of Baker [11], Karim *et al.* [5], Ray *et al.* [10] and the original experimental results of Mackay [12].

Table 1: Results Comparison

Results Comparison	Drag Coefficient (C_D)
Experimental [12]	0.00123 ±0.000314
Baker [11]	0.00167
Karim *et al.* [5]	0.00104
Ray *et al.*[10]	0.00153
Present Study	0.00119

For 3D model grid-independent solution test is carried out for the unstructured mesh of the solution domain. Table 2 shows variation of grid numbers do not affect results significantly. In general higher grid numbers give accurate resolution. But mesh size should be kept at minimum but sufficient value to reduce computational time. It is mentionable that, the computer having Processor- Intel(R) core(TM)2 Duo CPU E750@ 2.93GHz 2.94 GHz RAM- 2GB took around 25 hours to give optimum results of the model with ANSYS Fluent software version 16.2.

Table-2: Comparison of drag coefficient with experimental result for different number of unstructured grids

No. of Cells	No. of Nodes	Computed Drag Coefficient (C_D)	Experimental [12]
595385	123418	0.0011737878	0.00123 ±0.000314
714963	207031	0.001182085	
1012048	272602	0.0011985613	

5.0 RESULT AND DISCUSSION

Problem setup has been done on completion of grid generation. Flow is solved using the ANSYS Fluent software. Fig 5 shows residuals plot, where the solution is found convergent after completing 275 iterations. Fig 6 and Fig 7 show convergence history of drag and lift coefficients respectively.

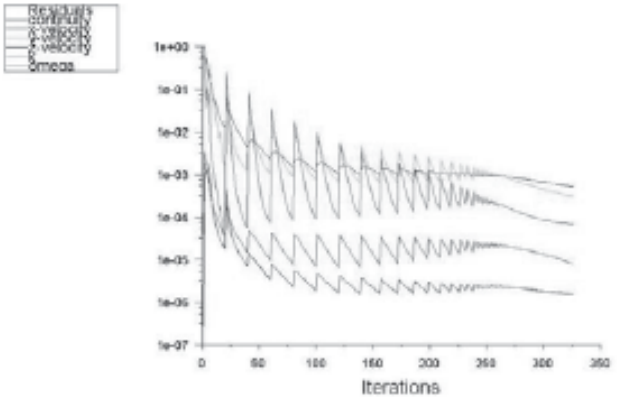

Fig 5: Residuals plot

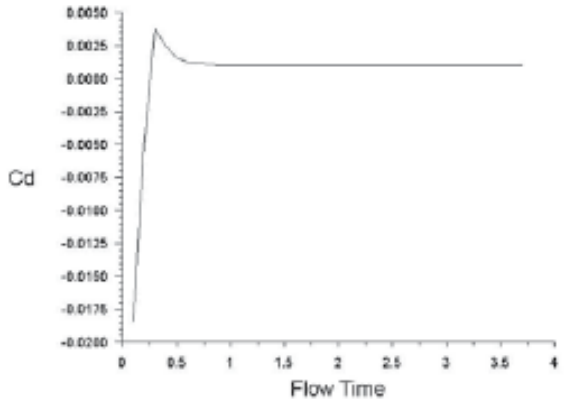

Fig 6: Drag coefficient (C_d) convergence history

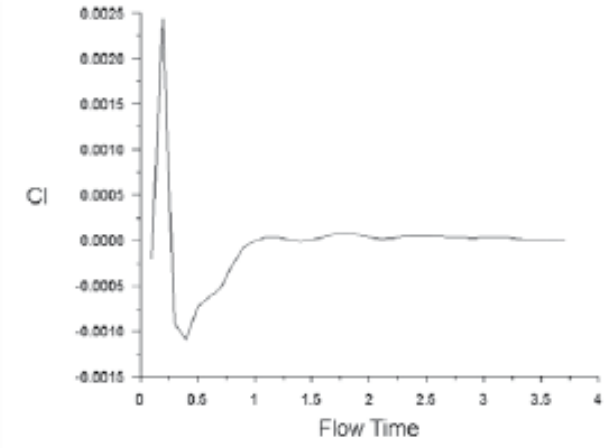

Fig 7: Lift coefficient (C_l) convergence history

Table 3 shows computed value of drag coefficient (C_d) around the body is 0.00119 for *Re* value 23003039 (velocity of 3.422 m/s). Viscous coefficient dominates pressure coefficients because of large body. Flux imbalance between inlet and outlet is found less than 1%.

Table 3: Numerical Results

Reynolds Number (*Re*)	23003039
Pressure Coefficient (C_p)	0.00046685576
Viscous Coefficient (C_v)	0.00073170558
Drag Coefficient (C_d=C_p+C_v)	0.0011985613
Flux Imbalance (kg/sec)	5.2970085e-07

Fig 8 shows the contours of static pressure around the body using unstructured grid. Fig 8(a) shows that total pressure field located in the longitudinal plane. The stagnation point of high pressure at the front tip, the favorable pressure gradient at the bow section and the adverse pressure gradient at the stern section of the DREA body are clearly shown. Fig 8(b) shows close-up view of the bow section. Stagnation point and the favorable pressure gradient are even more visible with red color. Fig 8(c) shows close-up view of the stern section.

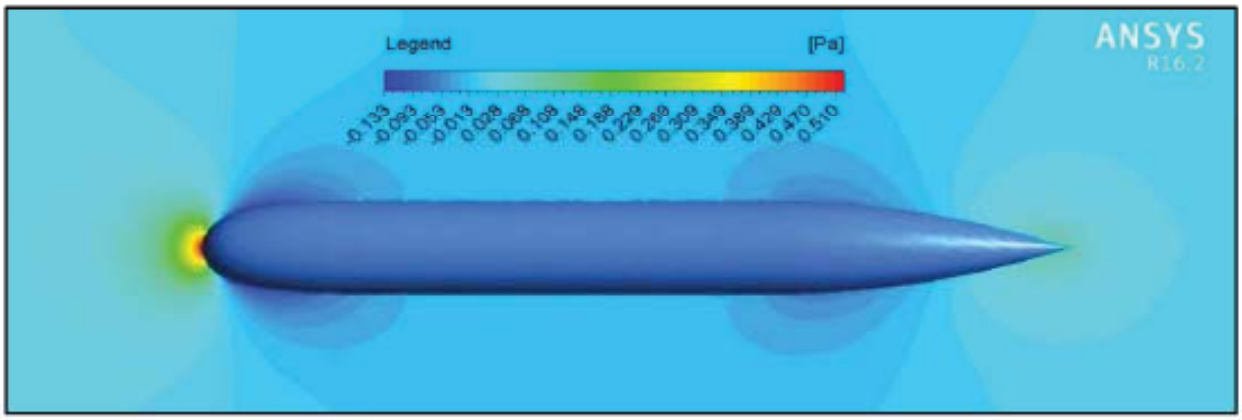

Fig 8(a): Pressure contours on xy plane of the domain

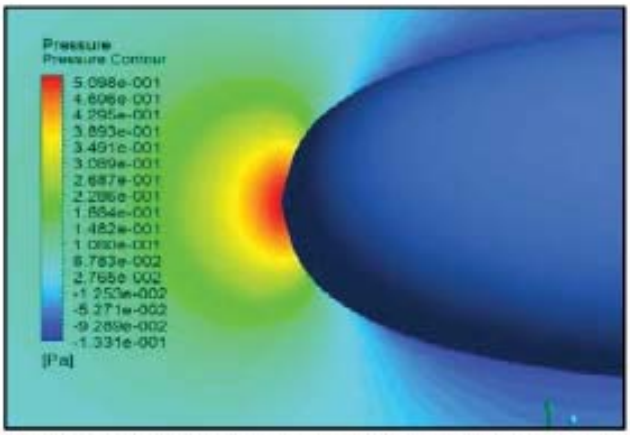

Fig 8(b): Enlarged view of pressure contours near at the bow

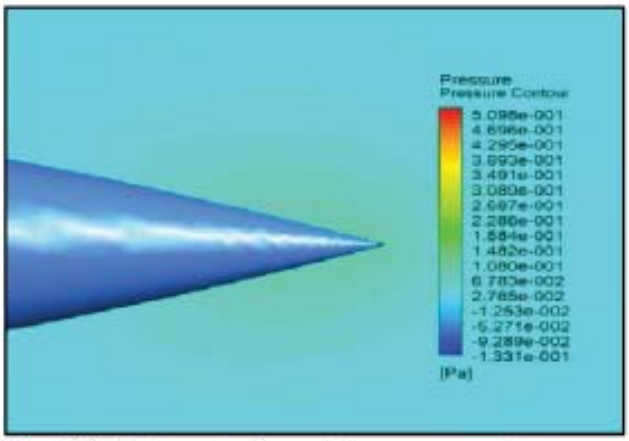

Fig 8(c): Enlarged view of pressure contours near at the stern

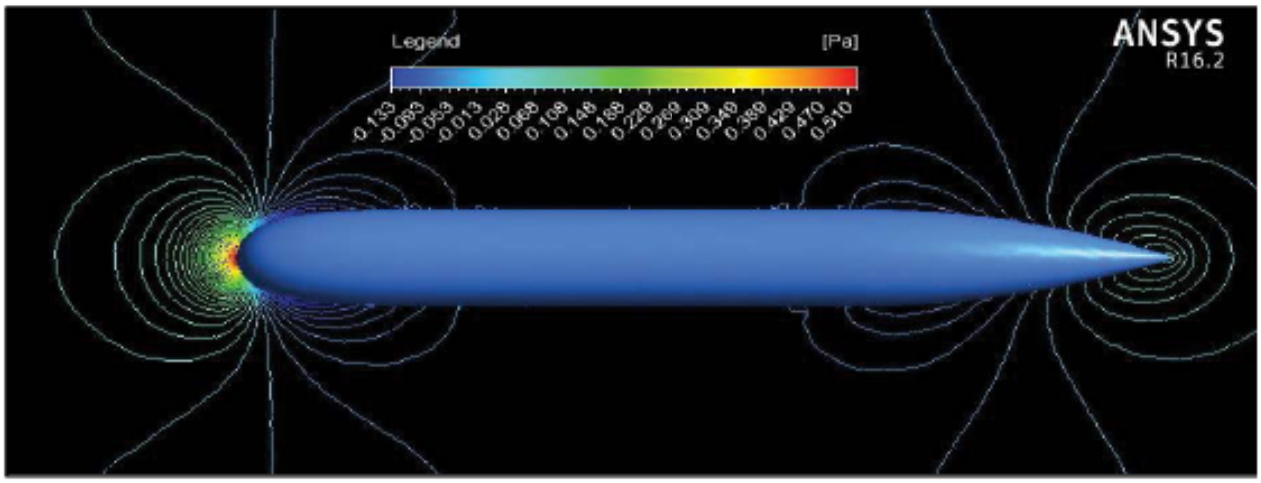

Fig 8(d): Pressure contours lines on xy plane of the domain

Overall the pressures at the bow and stern sections are higher compared to the pressure along the main DREA body.

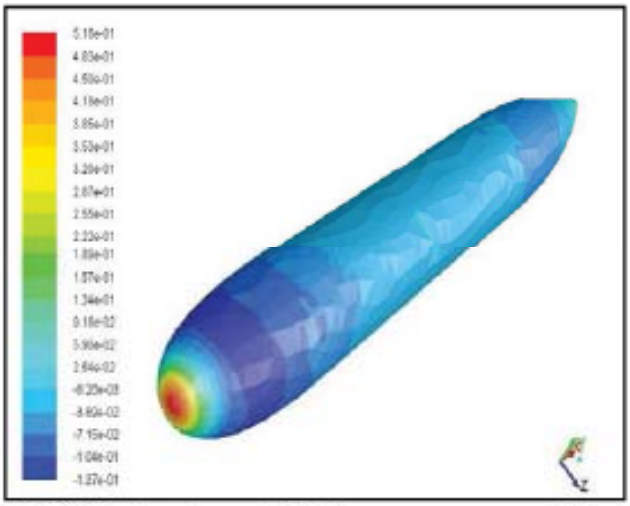

Fig8(e): Contours of static pressure around the body

Fig 9 shows the velocity distribution around the submarine body. It can be seen that the velocity near the nose is lower and the flow is accelerated as it reaches to the stern. This can be explained from the conservation of energy, an increase in the pressure of the fluid occurs simultaneously with a decrease in the velocity. As the pressure at the nose of the DREA is higher, therefore the velocity is lower (at stagnation point is actually a point with zero velocity) at this region. As the outlet gauge pressure is set to zero, and also due to the shape of tail, the flow-stream converges when it reaches to the stern and velocity increases.

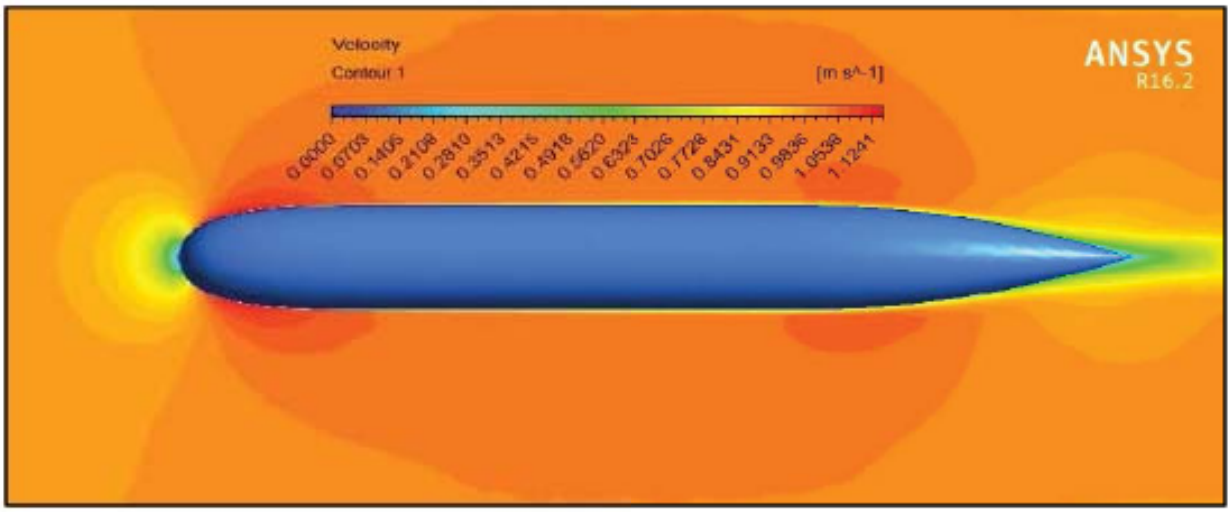

Fig 9(a): Velocity contours on xy plane of the domain

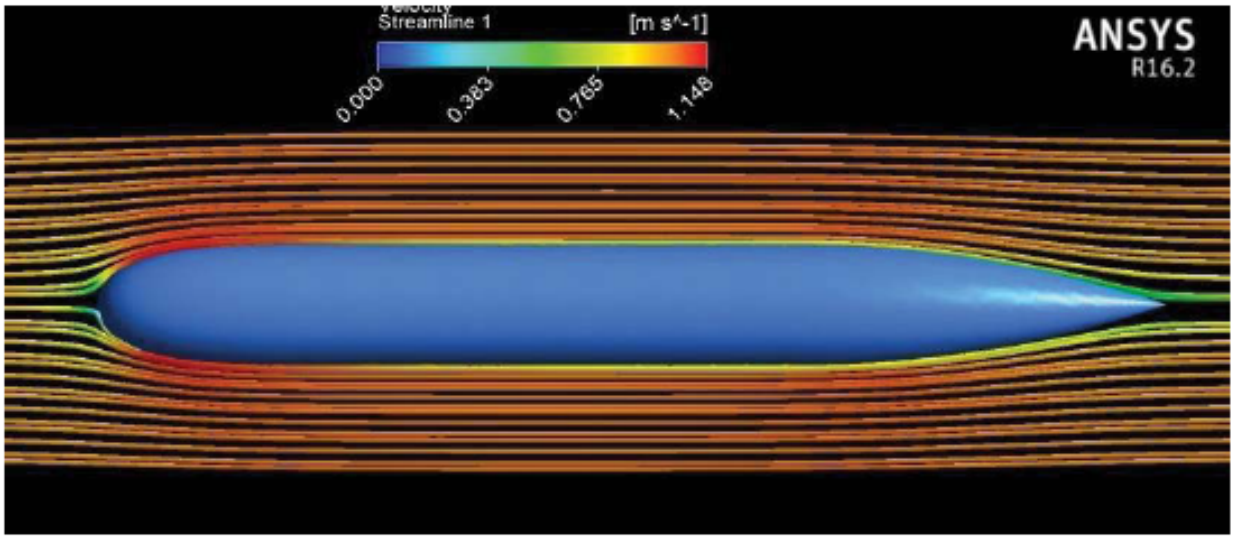

Fig 9(b): Velocity streamlines on xy plane of the domain

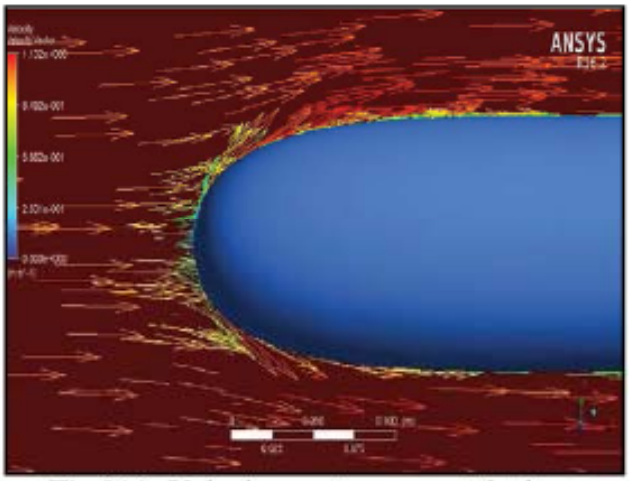

Fig 9(c): Velocity vectors near at the bow

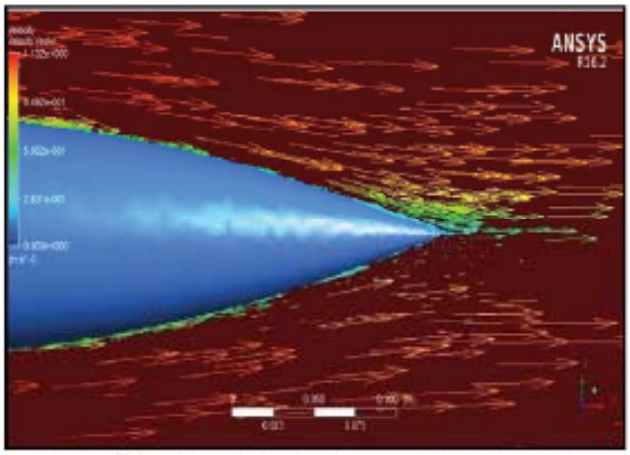

Fig 9(e): Velocity vectors near at the stern

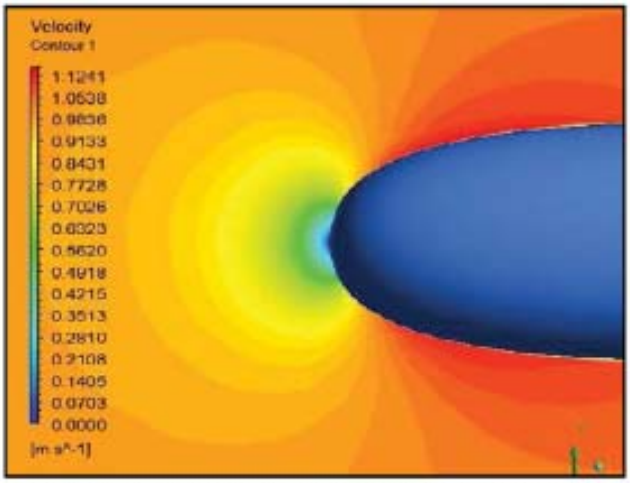

Fig 9(d): Enlarged view of velocity contour near at the bow

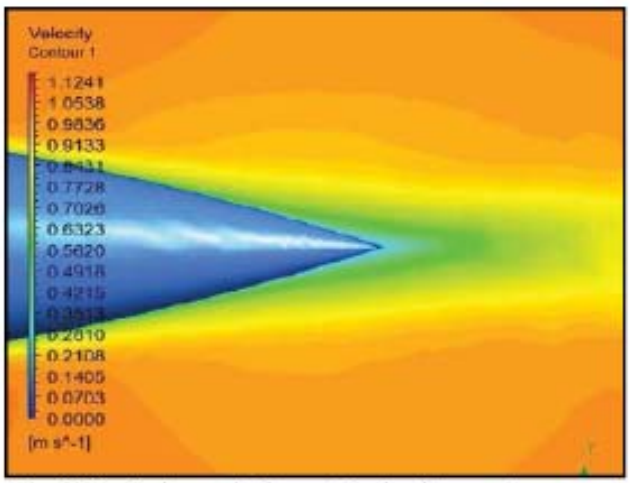

Fig 9(f): Enlarged view of velocity contour near at the stern

Fig 10(a) shows pressure coefficient (C_p) around the body. Due to the blunt edge, the highest pressure is found at bow area as expected. After that pressure decreases and becomes constant near the mid body. Near the aft body, the pressure decreases for a while and then moves up. Fig 10(b) shows variation of skin friction coefficient (C_f) around the body having opposite tendency compared to C_p which is usual. Fig 10(c) shows wall shear stress having similar trend of the curve of skin friction coefficient. Fig 10(d) shows variation of specific dissipation rate (ω) around DREA body. Turbulence increases both at leading and tailing edge and remain constant around mid body.

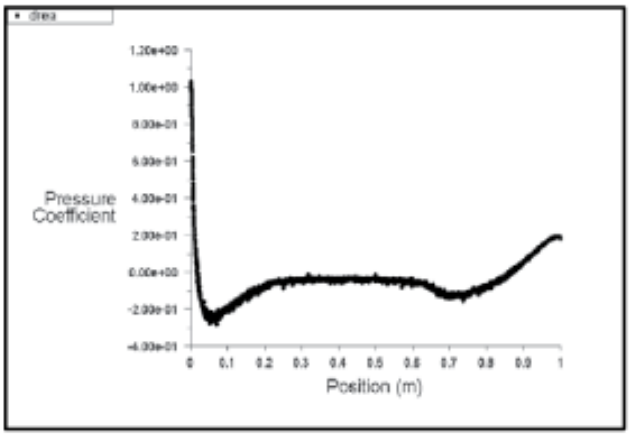

Fig 10(a): Variation of pressure coefficient (C_p) around DREA hull

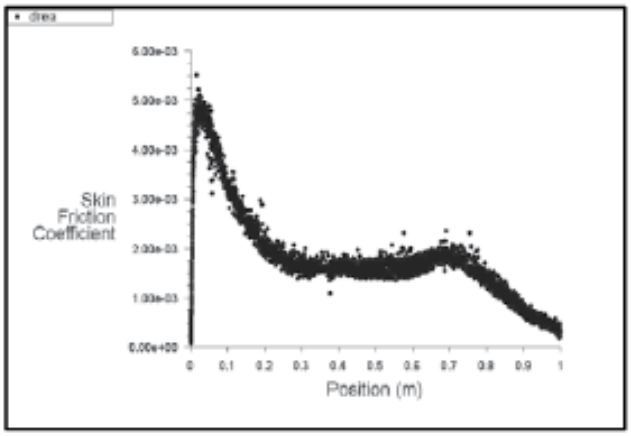

Fig 10(b): Variation of skin friction coefficient (C_f) around DREA hull

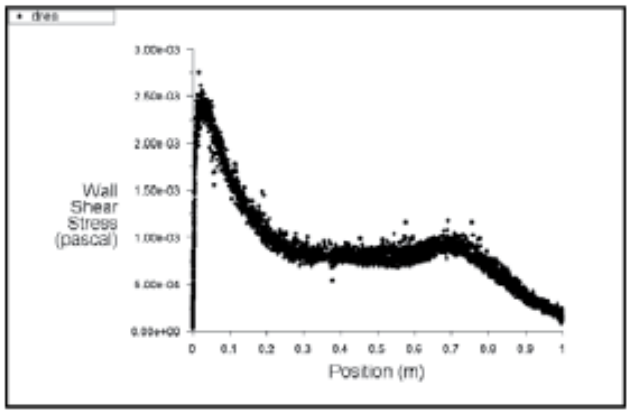

Fig 10(c): Variation of wall shear stress (τ_w) around DREA hull

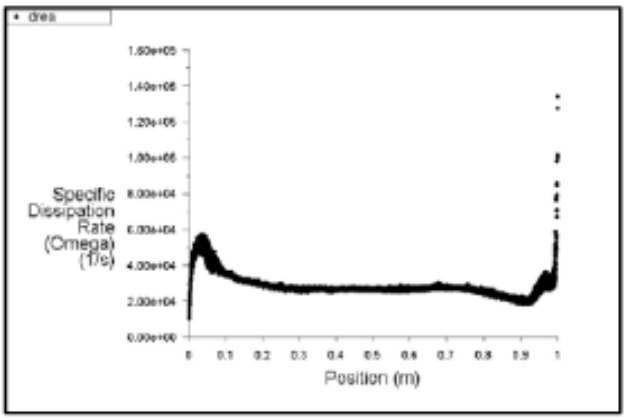

Fig 10(d): Variation of specific dissipation rate (ω) around DREA hull

6.0 CONCLUSION

In this study, flow around DREA bare submarine hull has been analyzed. Unstructured grid for the box type domain around 3D hull at zero angle of attack and SST k-ω turbulent model is used. Obtained results show good agreement with experimental and other researchers' results. The result of this study is important for understanding the flow visualization around the submarine shaped bodies that can be useful for improving design of autonomous underwater vehicles. Also the results show that numerical methods can be employed for estimation of the drag forces acting on 3D submarine shaped underwater bodies within reasonable accuracy. This estimation on drag force is useful for the calculation of power requirements at the early stage of design. In future, the simulation on similar types of body may be carried out with structured mesh and at various angles of attacks.

References

[1] V. C. Patel and H. C. Chen, Flow over tail and in wake of axisymmetric bodies: review of the state of the art, Journal of Ship Research, Vol. 30, No. 3, pp. 202-314 (1986).

[2] S. K. Choi and C. J. Chen, Laminar and turbulent flows past two dimensional and axisymmetric bodies, Iowa Institute of Hydraulic Research, IIHR Report 334-II (1990).

[3] T. Sarkar, P. G. Sayer, S. M. Fraser, A study of autonomous underwater vehicle hull forms using computational fluid dynamics, International Journal for Numerical Methods in Fluids, Vol. 25, pp. 1301-1313 (1997).

[4] C. K. G. Lam and K. Bremhorst, A modified form of the k-ε model for predicting all turbulence, ASME Journal Fluid Engineering, Vo.103, pp. 456 (1981).

[5] M. M. Karim, M. M. Rahman and M. A. Alim, Numerical computation of viscous drag for axisymmetric underwater vehicles, JurnalMekanikal, 26, 9-21 (2008).

[6] M. M. Karim, M. M. Rahman and M. A. Alim, Effectiveness of two-equation Eddy-Viscosity turbulence models for calculation of flow over underwater bodies of revolution, Southeast University Journal of Science and Engineering, Vol. 2, No.2 (2008).

[7] M. M. Karim, M. M. Rahman and M. A. Alim, Computation of turbulent viscous flow around submarine hull using unstructured grid, Journal of Ship Technology, ISSN: 0973-1423, Vol. 5, No. 1, pp. 38-52 (2009).

[8] M. M. Karim, M. M. Rahman and M. A. Alim, Performance of SST k-ω turbulence model for computation of viscous drag of axisymmetric underwater bodies, IJE Transactions B: application, Vol. 24, No. 2, 139-146 (2011).

[9] H. K. Versteeg and W. Malalasekara, An Introduction to Computational Fluid Dynamics- The Finite Volume Method, Longman Scientific & Technical, England (1995).

[10] J. Anderson, Computational Fluid Dynamics, McGraw-Hill, Inc., New York, 1995.

[11] C. Baker, Estimating Drag Force on Submarine Hulls, Contract Report, DRDC Atlantic CR 2004-125, Canada, (2004).

[12] M. Mackay, Flow visualization experiments with submarine models in a wind tunnel, Defence Research Establishment Atlantic, Canada (1988).

[13] ANSYS Fluent Theory Guide, Release 15.0, ANSYS, Inc., Canonsburg (2013).